

A random-walk model for dark matter halo spins

Andrew Benson^{1*}, Christoph Behrens², Yu Lu¹

¹ *Carnegie Observatories, 813 Santa Barbara Street, Pasadena, CA 91101, USA*

² *Institut für Astrophysik, Georg-August Universität Göttingen, Friedrich-Hundt-Platz 1, 37077, Göttingen, Germany*

14 January 2022

ABSTRACT

We extend the random-walk model of Vitvitska et al. for predicting the spins of dark matter halos from their merger histories. Using updated merger rates, orbital parameter distributions, and N-body constraints we show that this model can accurately reproduce the distribution of spin parameters measured in N-body simulations when we include a weak correlation between the spins of halos and the angular momenta of infalling subhalos. We further show that this model is in approximate agreement with the correlation of the spin magnitude over time as determined from N-body simulations, while it slightly underpredicts the correlation in the direction of the spin vector measured from the same simulations. This model is useful for predicting spins from merger histories derived from non-N-body sources, thereby circumventing the need for very high resolution simulations to permit accurate measurements of spins. It may be particularly relevant to modeling systems which accumulate angular momentum from halos over time (such as galactic discs)—we show that this model makes small but significant changes in the distribution of galactic disc sizes computed using the GALACTICUS semi-analytic galaxy formation model.

Key words: dark matter – large-scale structure of Universe – cosmology: theory

1 INTRODUCTION

The angular momenta of dark matter halos has long been understood to arise through tidal torques acting on the proto-halo (Hoyle 1949; Peebles 1969; Doroshkevich 1970; White 1984; Barnes & Efstathiou 1987; Porciani et al. 2002). These torques also impart angular momentum to the baryonic component of forming halos, and this is later incorporated into galaxies. Simple models, based on the assumption that material collapsing to form galactic discs conserves its original angular momentum, predict sizes of galactic discs in approximate agreement with observations Fall & Efstathiou (1980; see also Mo et al. 1998, but see Jiang et al. 2018 who show that galactic angular momentum is in fact not well correlated with halo spin, at least at zero time lag).

The angular momentum of halos, typically characterized by the dimensionless spin parameter, λ , has been measured directly from N-body simulations (Cole & Lacey 1996; Bett et al. 2007; Gottlöber & Yepes 2007; Macciò et al. 2007; Zhang et al. 2009; Lee et al. 2016; Rodríguez-Puebla et al. 2016; Zjupa & Springel 2017). However, Benson (2017a; see also Trenti et al. 2010) showed that spins are often poorly determined in N-body simulations because of particle noise—a 10% precision measurement of λ requires at least 50,000

bound particles in a halo. As the majority of halos found in cosmological N-body simulations will contain far fewer particles than this, their spin measurements will be unreliable.

An alternative approach is to predict halo formation histories from some other approach (e.g. those based on extended Press-Schechter theory), and assign spins to halos in those merger trees in some way. While the distribution of spins is known from N-body simulations (and is largely independent of mass and redshift), and the particle noise present in it can be “deconvolved” (Benson 2017a), assigning spins at random from this distribution is not a good approach as we expect spin to be correlated over some timescale at least of order the dynamical time of the halo, and possibly much longer. Cole et al. (2000) attempted to overcome this problem by drawing a spin at random from the measured distribution, but then assuming that this spin remained unchanged until a halo had grown in mass by a factor of 2, at which point a new spin was randomly drawn. This approach ensures correlation in spin across time, but is not well-motivated and its correlation structure has not been tested. Vitvitska et al. (2002; see also Benson & Bower 2010) proposed an alternative model based on the orbital angular momenta of merging halos (an idea also supported by the work of Bailin & Steinmetz 2005). Briefly, the angular momentum of any halo is tracked by following the contribution of spin and orbital angular momenta from each halo which

* E-mail: abenson@carnegiescience.edu

merges with it¹. Vitvitska et al. (2002) show that this model can reproduce the measured distribution of spin parameters, its independence on mass and redshift, and the enhancement in spin for halos with recent major mergers.

In this work, we develop their model further, by using up to date (and accurately calibrated) models for merger tree construction, halo concentrations, and distributions of orbital parameters for merging halos. We also consider the effects of unresolved accretion, and allow for the possibility of correlation between the angular momenta of infalling satellites and their host halo. This model is then calibrated to the distribution of spins measured in N-body simulations (accounting for particle noise), and the correlation structure of the calibrated model is explored.

2 METHODS

In this work we make use of two different definitions of spin parameter. The Vitvitska et al. (2002) model directly predicts halo angular momenta, making it simple to compute the corresponding spin under either definition. When constraining the model to match the distribution of spin parameters measured in the Millennium Simulation by Bett et al. (2007) (see §2.2) we utilize the Peebles (1969) definition of spin, as was employed by Bett et al. (2007):

$$\lambda_{\text{P}} = \frac{J|E|^{1/2}}{GM^{5/2}}, \quad (1)$$

where J is the magnitude of the halo’s angular momentum, E is the energy of the halo (consisting of both gravitational potential and kinetic energy), and M is the halo mass. When examining correlations in spin across time (see §3.2) we utilize the Bullock et al. (2001) definition of spin parameter:

$$\lambda_{\text{B}} = J/\sqrt{2}Mv_r, \quad (2)$$

where $v^2 = GM/r$ with r being the virial radius of the halo. This form is straightforward to compute from data available in the Millennium Simulation database (which does not directly provide halo energies; Lemson & Virgo Consortium 2006). As in the above two equations, we will use subscripts P and B to distinguish spins computed using the Peebles and Bullock definitions respectively.

The energy, E , of a halo (needed to compute the spin parameter under the Peebles (1969) definition) depends on the density profile of the dark matter halo. Throughout this work we assume NFW (Navarro et al. 1997) density profiles, and compute their concentrations using the method of Ludlow et al. (2016) as specifically implemented by Benson et al. (2019).

2.1 Model for halo spin

Our model closely follows that of Vitvitska et al. (2002). Specifically, we begin by building a merger tree using the algorithm of Parkinson et al. (2008) with parameters taken

from the posterior distribution found by Benson et al. (2019). While Vitvitska et al. (2002) used a fixed mass resolution when building their trees we instead adopt a resolution, M_{res} , which scales with the mass, M_0 , of the $z = 0$ halo in each tree—specifically, we set $M_{\text{res}} = 10^{-3}M_0$. This choice allows the most massive halos to be processed much more rapidly (as is necessary to facilitate the Markov Chain Monte Carlo (MCMC) simulation described in §2.2), while ensuring that all $z = 0$ halos are sufficiently well resolved to have robustly determined spin parameters. We have checked that increasing the resolution (e.g. to $M_{\text{res}} = 10^{-4}M_0$) makes no significant difference to our results; we find that the distribution of spin parameters for λ_{P} shifts by less than 0.02 dex for $\lambda_{\text{P}} < 0.1$ relative to the $M_{\text{res}} = 10^{-3}M_0$ case, and shifts by less than 0.05 dex for $\lambda_{\text{P}} < 0.2$. We then visit each halo in the tree in a depth-first manner (i.e. visiting all progenitors of a halo before visiting that halo itself) and compute a spin for that halo as follows:

- *Halos with progenitors:* For halos with one or more progenitors, each such progenitor will already have a spin parameter (and, therefore, an internal angular momentum) assigned. For non-primary progenitors (i.e. those which will merge with the primary progenitor and become subhalos) we assign orbital parameters at the point of merging as described in §2.1.1. We then simply sum the spin and orbital angular momenta in the centre of mass frame of the primary-secondary progenitor system. We allow for the orbital angular momentum to be divided by a factor $(1 + M_2/M_1)^{1-\epsilon}$, where M_1 and M_2 are the masses of the primary and secondary progenitors respectively, to allow for the possibility that orbital angular momentum is not conserved in the merger². We treat ϵ as a parameter of the model to be determined.

Since our merger trees have a finite mass resolution some accretion onto halos will be unresolved. With higher resolution this unresolved accretion would break up into low mass progenitor halos which would contribute to the angular momentum of each halo. To account for angular momentum contributed by these “sub-resolution” halos we assume that such unresolved accretion contributes angular momentum at the mean rate found by averaging over the orbital parameter distribution as described in §2.1.1. The contribution made to the angular momentum by sub-resolution halos will depend on the mass of those halos. This mass dependence arises from the $(1 + M_2/M_1)^{1-\epsilon}$ factor above, where M_2 is the mass of the sub-resolution halo. We therefore average the mean angular momentum (see §2.1.1) of sub-resolution halos, including this factor, over the mass function of sub-resolution halos. We assume a mass function slope of $\alpha = -1.9$ (Springel et al. 2008) for sub-resolution halos. The resulting angular momentum due to accretion of sub-resolution halos is then

$$J_{\text{unresolved}} = \frac{2 - \alpha}{\mu^{2-\alpha}} B(\mu/[1 + \mu]; 2 - \alpha, \epsilon - 2 + \alpha) M_{\text{unresolved}} \langle j \rangle, \quad (3)$$

where $B(x; a, b)$ is the incomplete beta function, $M_{\text{unresolved}}$ is the mass accreted in sub-resolution halos, and $\langle j \rangle$ is the mean specific orbital angular momentum of sub-resolution

¹ The physical origin of angular momentum remains the same as those merging halos gain their orbital angular momentum from large-scale tidal fields.

² Since mass can be lost from halos during major mergers (Lee et al. 2018) angular momentum may also be lost.

halos (see §2.1.1). In Appendix A we show that our results are well-converged with respect to resolution.

- *Progenitorless halos:* For halos with no progenitor we assign a spin parameter by drawing at random from a distribution—specifically we use the functional form of Bett et al. (2007) with parameters taken from the posterior distribution found by Benson (2017a).

Applying this procedure to a merger tree results in a determination of the internal angular momentum of each halo—these can be converted to spins following the usual definition (equations 1 and 2).

2.1.1 Orbital parameters of progenitor halos

Orbital parameters of merging halos are drawn from the distributions reported by Jiang et al. (2015), including the dependence on primary halo mass and secondary/primary halo mass ratio. The Jiang et al. (2015) results give the radial and tangential velocities of each merging secondary halo as it crosses the virial radius of the primary halo³. This specifies three of the six phase-space coordinates of the secondary halo. Previous works (Vitvitska et al. 2002; Benson & Bower 2010) have fixed the remaining three parameters by assuming that merging secondaries are distributed uniformly over the virial sphere of their primary, and that tangential velocities are isotropically distributed⁴. We move beyond this assumption and allow for the possibility of some correlation in the orbital parameters of secondaries. Specifically, we allow for a correlation between the orbital angular momentum, \mathbf{J}_{orb} , of the secondary, and the vector spin⁵, λ_{P} , of the primary, such that the angle θ between these two vectors is distributed as:

$$P(\cos \theta) = \frac{1}{2} (1 + \alpha |\lambda_{\text{P}}| \cos \theta), \quad (4)$$

where α is a parameter which controls the strength of the correlation⁶, and which we treat as a parameter of the model to be determined. Recently, An et al. (2020) have shown a strong anisotropy in the spin-orbit alignment of merging pairs of halos of comparable masses (mass ratios of 3 : 1 or less), with a distribution function similar in form to eqn. (4).

To sample orbits from this distribution we first draw orbital parameters from the distribution of Jiang et al. (2015),

³ We note that Jiang et al. (2015) adopt a definition of virial radius corresponding to the radius enclosing a mean interior density of 200 times the critical density. As this differs from that definition used in building our merger trees—which assume a spherical collapse model for defining the virial radius—we propagate the orbital velocities drawn from the Jiang et al. (2015) distribution to our preferred definition of virial radius assuming that energy and angular momentum are conserved along the orbit.

⁴ Vitvitska et al. (2002) examined the orbital parameters of infalling subhalos in cosmological N-body simulations but found no significant correlations. However, as they noted, given the statistical power of their sample such correlations could still be present at the level of 10–20%.

⁵ That is, a vector with magnitude equal to the spin parameter, and direction coincident with the internal angular momentum vector of the halo.

⁶ For $\alpha |\lambda_{\text{P}}| > 1$ this function becomes negative, making it an invalid distribution. In practice we find that this does not occur for values of α required to fit N-body simulations—see Appendix B.

and choose the remaining phase space coordinates assuming isotropically distributed infall on the virial sphere and isotropically distributed tangential velocities. We compute the resulting angular momentum vector, and from it determine $\cos \theta$. We then use rejection sampling, by accepting the orbit with probability

$$P(\cos \theta) = \frac{1 + \alpha |\lambda_{\text{P}}| \cos \theta}{1 + \alpha |\lambda_{\text{P}}|}, \quad (5)$$

to produce a distribution consistent with equation (4).

Since eqn. (4) depends only on the angle θ it is clear that the mean specific angular momentum of infalling halos must be aligned (or anti-aligned) with λ_{P} . For any given infalling halo the magnitude of its specific angular momentum along the direction of λ_{P} will be $j = r_{\text{v}} v_{\phi} \cos \theta$. Given the distribution in equation (4) the mean specific angular momentum of infalling halos is therefore

$$\langle j \rangle = \int_0^{\infty} dv_{\phi} \int_{-1}^{+1} d(\cos \theta) r_{\text{v}} v_{\phi} f(v_{\phi}) \cos \theta P(\cos \theta), \quad (6)$$

where $f(v_{\phi})$ is the distribution of the tangential component of orbital velocity of infalling halos. This integral is easily evaluated to give

$$\langle j \rangle = \frac{\alpha}{3} r_{\text{v}} \lambda_{\text{P}} \langle v_{\phi} \rangle, \quad (7)$$

where $\langle v_{\phi} \rangle = \int_0^{\infty} dv_{\phi} v_{\phi} f(v_{\phi})$ is the mean tangential velocity for infalling halos which we computed using the distribution of Jiang et al. (2015). Given the distribution in equation (4) the mean specific angular momentum of infalling halos is $\langle j \rangle = \alpha \lambda_{\text{P}} \langle v_{\phi} \rangle / 3$ where $\langle v_{\phi} \rangle$ is the mean tangential orbital velocity from the distribution of Jiang et al. (2015).

2.2 Constraining parameters of the model

The process described in the preceding sub-section is repeated for a large number of merger trees, using cosmological parameters and a power spectrum matched to the Millennium Simulation (Springel et al. 2005), $z = 0$ halo masses drawn from a Sheth et al. (2001) mass function (with parameters given by Benson et al. 2019) and spanning the range $3.53 \times 10^{11} M_{\odot}$ to $1.00 \times 10^{15} M_{\odot}$ to match the selection used by Bett et al. (2007). Bett et al. (2007) used a “quasi-equilibrium” criterion, based on the virial ratio $2T/U + 1$ (with T and U being the kinetic and potential energies of the halo respectively) to remove halos from their sample which were far from virial equilibrium. Since we can not compute the dynamical evolution of the virial ratio of halos in our model we instead remove halos which are likely to be unrelaxed based on a major merger criterion. Specifically, we exclude from our sample any $z = 0$ halo which experience a merger with mass ratio $M_2/M_1 > f_{\text{major}}$ more recently than a look-back time of t_{major} . We treat f_{major} and t_{major} as nuisance parameters when constraining the parameters of our model.

The spin of each remaining $z = 0$ halo computed in this way is convolved with the distribution function describing the effects of particle noise on measurement of N-body halo spins using the model of Benson (2017a). The quasi-equilibrium selection criterion that Bett et al. (2007) imposed on their halo sample was designed to remove any halos which are far from virial equilibrium. The model of Benson

(2017a) contains a log-normal component which models deviations of the mass and energy of an N-body halo from their true values due to particle noise. Any halos which experience a very large deviation in energy because of particle noise would be excluded from the Bett et al. (2007) sample by their quasi-equilibrium criterion. Therefore, when convolving halo spins with the Benson (2017a) distribution function we truncate the log-normal component beyond values that are a factor R above or below the mean. In this way we avoid populating the tails of the distribution which would correspond to halos excluded by the quasi-equilibrium criterion. We allow some freedom in the factor R as will be discussed below.

The results are summed over all merger trees to give the final distribution of spin parameters as would be measured in the Millennium Simulation using the approach of Bett et al. (2007). We then compute the likelihood of N-body results of Bett et al. (2007) given our model using:

$$\log \mathcal{L} = -\frac{1}{2} \Delta \mathbf{C}^{-1} \Delta^T, \quad (8)$$

where Δ is a vector of differences between the spin distribution of Bett et al. (2007) and that predicted by our model. The covariance matrix, $\mathbf{C} = \mathbf{C}_{\text{N-body}} + \mathbf{C}_{\text{model}}$, where the covariance matrix of the N-body data, $\mathbf{C}_{\text{N-body}}$, is assumed to be diagonal and equal to the Poisson variance in each bin, and the covariance matrix of our model calculation, $\mathbf{C}_{\text{model}}$, is computed following the approach of Benson (2014) accounting for the correlations introduced between bins by the process of convolving with the particle noise distribution.

The parameters of our spin model are then calibrated by running a MCMC simulation, following the approach of Benson (2017b) in detail, including utilizing the same MCMC algorithm and convergence criteria. Briefly, we perform a differential evolution MCMC simulation (Terr Braak 2006) using 128 parallel chains. At each step of the simulation a proposed state, S'_i , for each chain, i , is constructed by selecting at random (without replacement) two other chains, m and n , and finding

$$S'_i = S_i + \gamma(S_m - S_n) + \epsilon, \quad (9)$$

where γ is a parameter chosen to keep the acceptance rate of proposed states sufficiently high, and ϵ is a random vector each component of which is drawn from a Cauchy distribution with median zero and width parameter set equal to 10^{-9} of the current range of parameter values spanned by the ensemble of chains to ensure that the chains are positively recurrent. For a multivariate normal likelihood function in N dimensions the optimal value of γ is $\gamma_0 = 2.38/\sqrt{N}$ (Terr Braak 2006). We use this as our initial value of γ , but adjust γ adaptively as the simulation progresses to maintain a reasonable acceptance rate. The proposed state is accepted with probability P where

$$P = \begin{cases} 1 & \text{if } \mathcal{L}(S'_i) > \mathcal{L}(S_i), \\ \mathcal{L}(S'_i)/\mathcal{L}(S_i) & \text{otherwise,} \end{cases} \quad (10)$$

and where \mathcal{L} is the likelihood function.

The simulation is allowed to progress until the chains have converged on the posterior distribution as judged by the Gelman-Rubin statistic, \hat{R} (Gelman & Rubin 1992), after outlier chains (identified using the Grubb's outlier test (Grubbs 1969; Stefansky 1972) with significance level

$\alpha = 0.05$) have been discarded. Specifically, we declare convergence when $\hat{R} = 1.2$ in the parameters of interest, ϵ and α .

The Gelman-Rubin convergence measure relies on the chains be initialized in an over dispersed state. The state of each chain is therefore initialized by constructing 128-point unit Latin hypercubes. We generate 100 such cubes and find the cube which maximizes the minimum (ℓ^2 -norm) distance between any two points in the hypercube. Each point in this hypercube realization is used as the initial state for a chain by associating $C_i = L_i$ where L_i is the i^{th} coordinate of the point in the hypercube, and C_i is the cumulative probability distribution of the prior on parameter i . The parameter values are then simply found by inverting their cumulative distributions.

We allow the following parameters to vary in this MCMC simulation:

- (A, a, p) in the Sheth et al. (2001) mass function, $(G_0, \gamma_1, \gamma_2)$ in the halo merger rate model of Parkinson et al. (2008), and (f, C) in the halo concentration model of Ludlow et al. (2016) all as defined by Benson et al. (2019), with a multivariate normal prior matched to the posterior distribution found by Benson et al. (2019).
- $(\lambda_{P,0}, \alpha)$ in the spin parameter distribution fitting function⁷ of Bett et al. (2007), with a multivariate normal prior matched to the posterior distribution found by Benson (2017a).
- (b, γ, σ, μ) in each primary halo mass, and secondary-to-primary mass ratio in the fitting function for orbital parameters of subhalos of Jiang et al. (2015), with normal priors with means and variances derived from the best-fit values and errors reported by Jiang et al. (2015).
- The major merger mass ratio, f_{major} , and time, t_{major} , used to exclude halos with recent major mergers, with normal priors with (mean, variance) of (0.20, 0.01) and (0.50, 0.09) respectively. The prior for f_{major} is motivated by the fact that Bett et al. (2007) excluded halos with $|2T/U + 1| < Q$ with $Q = 0.5$. Perturbations of this magnitude to virial equilibrium should be expected to require mergers of mass ratio roughly comparable to Q . The timescale for exclude halos with recent major mergers is motivated by the study of Drakos et al. (2018) who find that virial equilibrium is reestablished within around 2 Gyr after first passage for binary (i.e. equal mass) mergers of typical $z = 0$ halos, we therefore expect a revirialization timescale shorter than this for major but non-binary mergers.
- The factor R at which the log-normal component of the Benson (2017a) particle noise distribution function is truncated to mimic the effects of the Bett et al. (2007) quasi-equilibrium selection criterion. We expect this factor to be $R \approx 1 + Q$, but allow some freedom by adopting a uniform prior in the range 1.4 to 2.0.
- ϵ in our model for the angular momentum retained by halos during mergers, with a uniform prior between 0 and 3. A value of $\epsilon = 1$ indicates no loss of angular momentum during mergers. Since major mergers can lead to mass loss, and therefore angular momentum loss, we may expect $\epsilon > 1$. Lee et al. (2018) find mass loss at the level of 10% following

⁷ This distribution is used to sample spin parameters for halos with no progenitors.

major ($M_2/M_1 > 0.3$) mergers. If 10% of angular momentum was lost in such cases it would imply $\epsilon \approx 1.4$. However, since mass is lost from the outer regions of halos it is likely that the specific angular momentum of the lost material is higher than average. The upper limit of our prior is therefore chosen to be sufficiently high to allow for the specific angular momentum to be enhanced by a factor of around 1.5 above the average. While the above arguments regarding angular momentum loss suggest $\epsilon > 1$ we allow our prior to extend to $\epsilon = 0$ —our model is idealized in several respects (e.g. it assumes spherical halos) so we allow for the possibility that a better match to the N-body results may be obtained with $\epsilon < 1$.

- α in our model for correlated infall orbits with a prior that is uniform in α between $\alpha = 0$ and 20. While Vitvitska et al. (2002) measured no correlations between orbital parameters of infalling satellites and their host halos, the small size of their sample left the possibility of a correlation at the 10–20% level. In our model for correlated orbits this would correspond to α in the range 2–3 for typical spin parameters. An et al. (2020) show results for approximately equal-mass mergers of halos which correspond to a much larger $\alpha \sim 20$. We allow a broad range of α which encompass these expectations.

This gives a total of 50 parameters, although most of them are well-constrained by previous analyses.

3 RESULTS

Our MCMC simulation reaches convergence (as judged by the Gelman–Rubin statistic—see §2.2) after 2,090 steps. We discard these initial burn-in steps then allow our MCMC simulation to run for a further 2,450 steps. The posterior distribution over the model parameters is then determined from those post-convergence steps. The correlation length in our chains is around 26 steps. Therefore, with 128 chains we have approximately 12,000 independent draws from the posterior distribution. We find that the parameters of our spin model are constrained to be $\epsilon = (2.40^{+1.20}_{-0.80}) \times 10^{-1}$ and $\alpha = (6.6^{+11.3}_{-4.5}) \times 10^{-1}$. The parameters controlling removal of halos with recent major mergers are constrained to be $f_{\text{major}} = (1.90^{+0.71}_{-1.06}) \times 10^{-1}$, $t_{\text{major}} = (2.8^{+4.3}_{-1.4}) \times 10^{-1}$ Gyr, and $R = 1.420^{+0.065}_{-0.022}$. The remaining nuisance parameters have posterior distributions largely consistent with their priors.

Interestingly the posterior distribution of ϵ is found to be almost entirely constrained to the $\epsilon < 1$ region, contradicting our expectation that angular momentum loss in major mergers would lead to $\epsilon > 1$. The posterior also favours a non-zero $\alpha \approx 0.9$ indicating that some correlation between subhalo orbits is preferred, although not as strong as that reported by An et al. (2020) for approximately equal-mass mergers. We find (see Appendix B) that ϵ and α are strongly correlated. We will comment further on this correlation and its implications in §3.2.

3.1 Spin distribution

Using the maximum posterior probability model found by our MCMC simulation we compute the $z = 0$ distribution of (Peebles) spin parameters for the halo mass range used

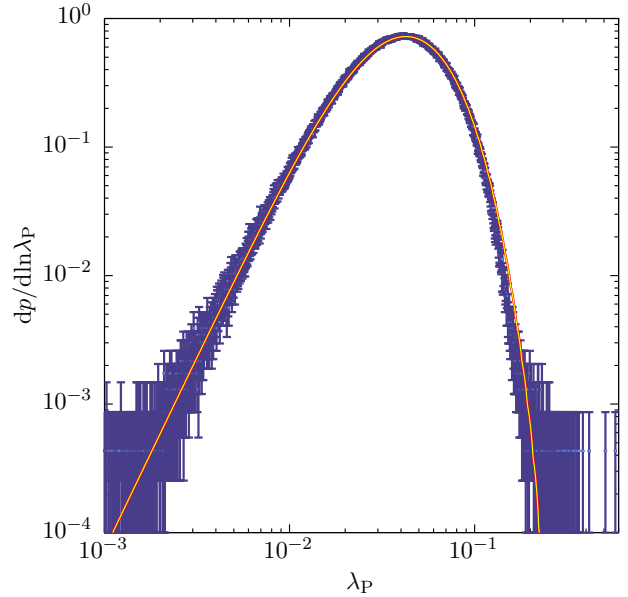


Figure 1. The distribution of spin parameters, λ_p , for relaxed halos at $z = 0$. The blue points with error bars show the results of Bett et al. (2007), while the yellow line shows the results from our model for the maximum posterior probability model after convolution with the particle noise distribution predicted by the model of Benson (2017a).

by Bett et al. (2007), convolve them with the particle noise distribution of Benson (2017a) and compare them with the distribution measured by Bett et al. (2007) for N-body halos. The results are shown in Figure 1.

It is apparent that our model matches the N-body results extremely well. In particular, the position of the peak in the distribution, the width of the distribution, and the low- λ_p slope are all almost perfectly reproduced. At high- λ_p our model slightly overpredicts the distribution function, although this is a regime where the details of how unrelaxed halos are rejected from the sample and the specifics of the particle noise distribution have the greatest effect. Less than 10% of halos have spins in this regime.

3.2 Correlations

To examine the correlation structure of the spin of a halo across time we first extract a set of merger trees with $z = 0$ halo masses in the mass range 3.53×10^{13} to $10^{15} M_\odot$ from the Millennium Simulation database. Halos in this mass range in the Millennium Simulation contain at least 30,000 particles, and so their spins are only mildly affected by particle noise. We compute spins for all halos in these trees under the Bullock et al. (2001) definition, and then extract the time series of spin along the main branch of the merger tree back to early times. We then measure the correlation of spin parameter magnitude of $z = 0$ halos with that of their progenitor at early times, and also measure the correlation of $\cos \theta$, where θ is the angle between the spin vectors of the $z = 0$ halo and its earlier progenitor.

At each look-back time the correlation functions are

computed by averaging over all $z = 0$ halos in our sample which have a resolved progenitor at that time. Therefore, the number of $z = 0$ halos averaged over at each look-back time will decrease as look-back time increases due to the fact that there is a maximal look-back time for each $z = 0$ halo at which a resolved progenitor halo exists. This will have two effects on the correlation function:

(i) The correlation function will become noisier at large look-back times due to the smaller number of $z = 0$ halos contributing (noise is also contributed at large look-back times by the fact that the progenitor halos consist of ever fewer particles, due to their decreasing masses, making their spins less well-determined);

(ii) Some bias may be introduced if, for example, the auto-correlation function, $\text{Corr}(|\lambda_P|)$ (the correlation between the magnitude of spin of the $z = 0$ halo and its progenitor at some earlier time), is itself correlated with halo formation history (which, in our model, it of course is) since trees which formed earlier will have larger maximal look-back times.

For comparison, we construct a sample of merger trees using the model described in this work using the maximum posterior probability model found by our MCMC simulation, spanning the same range of masses and in a cosmology matched to that of the Millennium Simulation. These merger trees are constructed with the mass halo mass resolution as those taken from the Millennium Simulation. As such, our merger trees have a distribution of maximal look-back times which is consistent with those from the Millennium simulation (as expected given that we use a merger tree building algorithm which has been calibrated to N-body simulation progenitor mass functions).

After computing angular momenta of each halo in these trees we use the model of [Benson et al. \(2019\)](#) to add noise to the angular momenta and masses of each halo to represent the effects of particle noise—while this is generally a small effect for halos containing 30,000 particles or more as in this sample we nevertheless account for the effects of this noise⁸. Our merger trees (to the extent that our model is a valid description of the physics governing halo spins) should have the same statistical and systematic uncertainties as the N-body data to which we compare. Finally, we compute the spin parameters of these halos under the [Bullock et al. \(2001\)](#) definition and compute correlations in spin magnitude and direction in the same way as for the Millennium Simulation halos.

Figure 2 shows the resulting correlation functions for the Millennium Simulation ([Springel et al. 2005](#)) and for our model. Considering first the correlation in the magnitude of spin (yellow lines), our model (dashed line) matches that measured in the Millennium Simulation (solid line) very well across the full range of look-back times, with only a slight over-estimation of correlation at look back times less than 6 Gyr. The dotted green line in Figure 2 shows the Galform model ([Cole et al. 2000](#)) in which spins are selected at random from a distribution, and updated each time a halo doubles its mass. It can be seen that this does not produce the correct correlation structure as measured from the Mil-

⁸ The noise becomes more significant for progenitor halos at early times which have significantly lower masses.

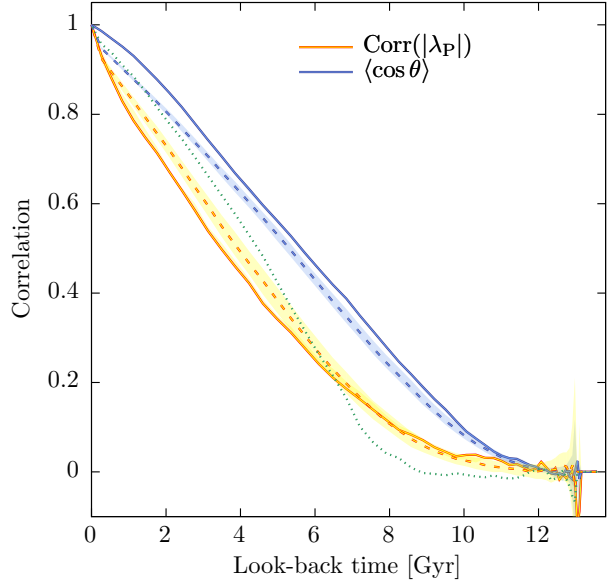


Figure 2. Correlation functions of spin magnitude (yellow lines) and angle (blue lines) from the Millennium simulation (solid lines), and from our model (dashed lines). For the Millennium simulation the line shows the result averaged over all halos, with the shaded region indicating the 10–90% inter-percentile region over all halos. For our model the line indicates the median from the posterior distribution, with the shaded region indicating the 10–90% inter-percentile region of the posterior distribution. The dotted green line shows the correlation function for spin magnitude in the Galform model ([Cole et al. 2000](#)) in which spins are selected at random, and updated each time a halo doubles its mass.

lennium Simulation, over-predicting the correlation up to look-back times of 6 Gyr, beyond which it underpredicts (at a level comparable to that underprediction found using the model in this work). We will briefly explore the consequences of these differences in §4.

In terms of the angle between the $z = 0$ spin vector and that at earlier times (blue lines), our model (dashed line) decorrelates somewhat faster than the N-body halos (solid line) with look-back time, but reproduces the overall trend, and matches the N-body correlation quite well for larger look-back times. This suggests that our model for the correlations between infalling subhalo orbits does not capture the true correlations sufficiently well.

Recently, [Morinaga & Ishiyama \(2019\)](#) examined the filamentary nature of subhalo accretion, finding correlations between the strength of filamentary accretion and halo shape and orientation. This clearly demonstrates that the correlations arising from the filamentary nature of accretion can have measurable effects on halo properties. They find that the angular momentum vectors of halos tend to be aligned perpendicularly with the direction of filaments (see also [Libeskind et al. 2012](#)).

Our model for correlated infall orbits was chosen to be simple and empirical, and, for example, does not explicitly account for the filamentary nature of subhalo accretion. The results shown in Figure 2 suggest that this model should be

improved, perhaps by studying these correlations directly in N-body simulations and developing a model to describe them. Furthermore, we find (see Appendix B) that the parameter describing correlated infall orbits is strongly correlated with the parameter ϵ which parameterizes the non-conservation of angular momentum in major mergers. We find $\epsilon < 1$ which implies that major mergers contribute more angular momentum than expected. An improved model for the correlated nature of infall orbits may therefore also change the inference for ϵ —a model which gave stronger correlation between the angular momentum vectors of infalling satellites and the spin of the host halo would presumably allow ϵ to increase, as the mean angular momentum per merger would then be larger. Alternatively, the inference of $\epsilon < 1$ may indicate that our model is too simplistic to capture the details of major merger events—examination of the angular momentum content of well-resolved cosmological N-body halos undergoing major mergers may shed light on this aspect of the model.

3.3 Further Tests

Utilizing the same sample of merger trees as in §3.2 we can construct further tests of how well our model matches measurements related to halo spin in N-body simulations. In the following we will explore how the spin depends on halo formation history, and examine the distribution of “spin-flips” (i.e. large changes in the direction of the spin vector).

3.3.1 Dependence on Halo Formation Time

We first consider how the median halo spin correlates with halo formation time, t_f . We adopt a conventional definition of formation time as that time at which the primary progenitor of a $z = 0$ halo first reaches 50% of the mass of that $z = 0$ halo. We compute formation times using the merger trees our model (i.e. built using the Parkinson et al. (2008) algorithm), and from the Millennium Simulation, using the same sample of $z = 0$ halos as in §3.2. We then compute the median spin parameter in bins of formation time.

Figure 3 shows the results of this analysis. There is a clear trend for the median spin to increase as formation time increases. Note that, in this analysis, we have not excluded any halos on the basis of recent mergers or departures from virial equilibrium. In the case of the Millennium Simulation (solid line), the median spin increases from close to $\bar{\lambda}_B = 0.020$ for halos formed at $t = 4$ Gyr, to $\bar{\lambda}_B = 0.054$ for halos formed very recently. Comparing the the posterior predictions from our model, we see that the trend is matched quite well for early-forming ($t_f < 9$ Gyr) halos, but for later-forming halos our model predicts no significant correlation between formation time and median spin.

Halos which formed recently are more likely to have recent major merger events than those which formed early. We therefore interpret the trend found in the N-body simulation as indicating that, on average, major mergers temporarily increase the halo spin, while extended periods of slow accretion (consisting of many minor mergers) cause a regression toward the mean and halo spin decreases. Our model fails to produce a sufficiently strong trend of median spin with formation time at late times. This may indicate that our

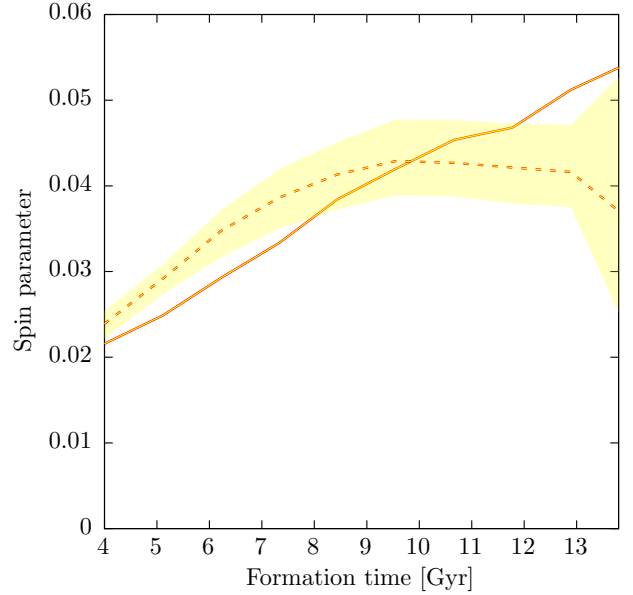


Figure 3. The median (Bullock) spin parameter for $z = 0$ halos as a function of halo formation time—defined as the time at which the primary progenitor of the $z = 0$ halo first reaches 50% of the mass. The solid line indicates results from the Millennium Simulation, while the dashed line and shaded region indicate the median and 10% and 90% percentiles of the posterior distribution from our model.

model has too many minor mergers/too few major mergers at late times (a known problem in the Parkinson et al. (2008) merger tree algorithm—see Benson (2017b; Fig. 7) for example).

3.3.2 Distribution of “Spin Flips”

We next examine the distribution of “spin-flips” (Bett & Frenk 2012), that is, the distribution of the change in angle of the spin vector over short time intervals. To examine this we measure the quantities:

$$\Delta\mu(t) = \frac{M(t) - M(t - \tau)}{M(t)}, \quad (11)$$

and

$$\cos\theta(t) = \frac{\mathbf{J}(t) \cdot \mathbf{J}(t - \tau)}{|\mathbf{J}(t)||\mathbf{J}(t - \tau)|}, \quad (12)$$

defined by Bett & Frenk (2012), and which measure the fractional change in the mass of a halo, and the change in the angle of the halo’s angular momentum vector over a timescale τ . Bett & Frenk (2012) choose $\tau = 0.5$ Gyr. We choose a value of $\tau = 0.54$ Gyr which is close to that of Bett & Frenk (2012) and corresponds precisely to an interval between snapshots of the Millennium Simulation and so avoids the need for any interpolation.

In Figure 4 we show the cumulative distribution of $\cos\theta$ for our sample of $z = 0$ halos, for subsamples with $\Delta\mu \geq 0$, 0.1, and 0.3 (yellow, blue, and green lines respectively). For the N-body simulation (solid lines) the distribution is

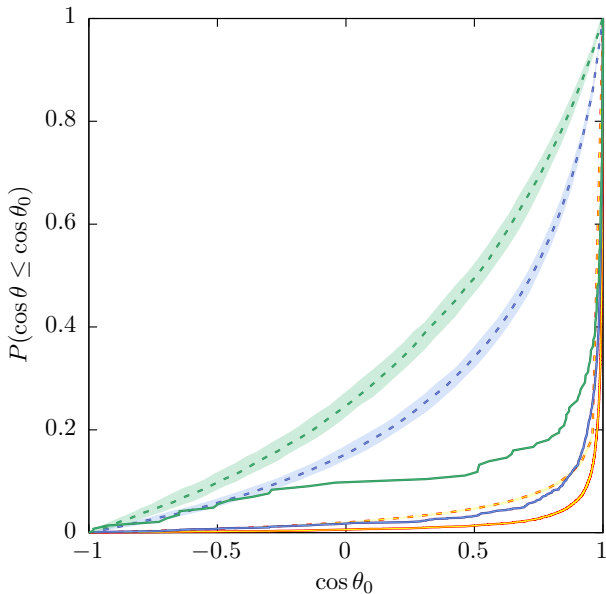


Figure 4. The cumulative distribution of spin-flip angles, θ , for halos at $z = 0$ measured over a time interval of 0.54 Gyr. Solid lines indicate results from the Millennium Simulation, while the dashed lines and shaded regions indicate the median and 10% and 90% percentiles of the posterior distribution from our model. The yellow, blue, and green lines show results for mass fraction changes of $\Delta\mu \geq 0, 0.1, \text{ and } 0.3$ respectively.

strongly concentrated around $\cos \theta = 1$ (i.e. no change in angle) with a long tail to smaller values. For larger $\Delta\mu$ (i.e. halos which have experienced significant recent mass growth) the distribution becomes more extended.

Comparing the results from our model we see that, for the $\Delta\mu > 0$ subsample the distribution of $\cos \theta$ is also strongly concentrated around $\cos \theta = 1$, although the tail to lower $\cos \theta$ is heavier. For the $\Delta\mu \geq 0.1, \text{ and } 0.3$ subsamples though our model predicts a significantly more extended tail. This difference from the N-body results is closely related to our finding of $\epsilon < 1$, which enhances the angular momentum provided by major mergers, and therefore causes such mergers to result in much larger changes in the direction of the angular momentum vector.

4 DISCUSSION

We have described an updated implementation of the random walk model for halo angular momentum first proposed by Vitvitska et al. (2002). Our approach utilizes updated algorithms for merger tree construction, more accurate distributions of orbital parameters, correlations between those parameters, and is carefully calibrated to measurements from N-body simulations accounting for the effects of particle noise. The resulting algorithm is implemented within the open-source semi-analytic model GALACTICUS⁹ and so is available for any one to use. We also provide an overview

of our algorithm in the form of a flowchart in Appendix C. The resulting model accurately reproduces the measured distribution of spin parameters from N-body simulations for $\lambda_p < 0.1$, slightly overpredicting the distribution at larger spins. Achieving this match requires non-zero correlations between the angular momenta of infalling halos and the spin of the halo with which they are merging. Although this can not be tested in our model, it is expected that these correlations derive from the large scale tidal field around the host halo which is coherent over cosmological timescales, and the filamentary nature of subhalo accretion.

Once calibrated to match the distribution of spin parameters in halos, the model can be used to explore correlations in spin parameter magnitude and direction over time in halos. We find that the model accurately matches the correlation measured from N-body simulations in the magnitude of the spin up to a look-back time of 4 Gyr, somewhat underpredicting the correlation at larger look-back times. The agreement with N-body results is significantly improved with respect to algorithms previously used in semi-analytic galaxy formation models (Cole et al. 2000). Correlation in the direction of the spin vector is somewhat underestimated with respect to measurements from N-body simulations, suggesting that our simple model for correlations in the orbital parameters of infalling subhalos is insufficient, and should be improved (perhaps by understanding developed from studies of N-body simulations). This point is further emphasized by considering the distribution of “spin flips” (Bett & Frenk 2012, 2016) in which our model shows much larger changes in the direction of the spin vector as a result of large mass accretion events than is found in N-body simulations. These and similar statistics will therefore provide a useful test of any improvements to our model resulting from further studies of correlations in the orbital parameters of infalling subhalos. We also find that our model qualitatively reproduces trends between spin parameter and halo formation time, although quantitative differences remain.

The random walk model described here allows for spins to be assigned to dark matter halos in merger trees in a manner that is internally consistent with their formation histories. Since halo concentrations are also known to correlate strongly with halo formation history (Ludlow et al. 2016) this model could be combined with that described by Benson et al. (2019) to explore correlations between spin, concentration, and environment (as examined by Johnson et al. 2019, for example). We intend to explore these correlations in a future work.

Perhaps most importantly, since this model approximately captures the correlation structure of halo spin (both its magnitude and direction) over time, this opens up the possibility of more accurately tracking angular momenta of halos and galactic discs in semi-analytic models of galaxy formation without the need for very high resolution N-body simulations¹⁰, or ad-hoc assumptions about when and how spins change. As a preliminary test of how galaxy sizes might

¹⁰ As shown by Benson (2017a) a 10% precision measurement of λ_p in an N-body halo requires that the halo be resolved with at least 50,000 particles. Since galaxies form over time as their halo grows this means that all progenitor halos in which the galaxy undergoes significant growth must also be resolved with a similarly large number of particles.

⁹ github.com/galacticusorg/galacticus

be affected by the use of this model we show in Figure 5 a comparison of the distribution of half-mass radii of galactic discs in disc-dominated central galaxies in $2 \times 10^{12} M_{\odot}$ halos at $z = 0$ as computed using the GALACTICUS semi-analytic model¹¹ (Benson 2012) using the “Galform” model¹² for spins (Cole et al. 2000), and using the model developed in this paper¹³. We find only small changes in the distribution of galaxy sizes when adopting the spin model developed in this work. Specifically the mean logarithm of disc half-mass radius increases from $\langle \log_{10}(r_{1/2}/\text{kpc}) \rangle = 0.529$ to 0.535, with the root-variance in logarithm of half-mass radius increasing from $\sigma_{\log_{10}(r_{1/2}/\text{kpc})} = 0.106$ to 0.120. These changes are small, which indicates that previous, simpler models for halo spin should likely not have led to significantly incorrect results. However, as the model described in this work provides a more detailed description of how the spin of halos evolves, semi-analytic models such as GALACTICUS should be updated to exploit this. For example, GALACTICUS currently does not make use of the vector nature of spin when computing the evolution of disc angular momentum. Accounting for the vector nature of spin will likely also change the resulting distribution of disc sizes. We leave exploration of these consequences of the model developed in this work to a future paper.

¹¹ This model for the sizes of galactic disks has its origins in the works of Fall & Efstathiou (1980) and Mo et al. (1998) and assumes that the angular momentum content of the galactic disk is directly related to that of the dark matter halo. Unlike those models, in which there is a perfect correlation between the instantaneous angular momentum of the disk and that of the host halo, in GALACTICUS (see also Cole et al. 2000) the angular momentum of the disk is accumulated over time as gas cools within each halo, and is further modified by feedback-driven outflows. As such, the disk angular momentum is not perfectly correlated with the instantaneous spin of the halo. Several works (Chen et al. 2003; Bett et al. 2010; Sharma et al. 2012; Bryan et al. 2013; Lu et al. 2015; Liao et al. 2017; Zjupa & Springel 2017; Jiang et al. 2019) have demonstrated significant deviations between the angular momentum content of dark matter and baryons in a halo. This may suggest that semi-analytic models for the sizes of galactic disks, such as that utilized here, require significant modification. Nevertheless, a reliable model for the spins of dark matter halos is likely to remain an important ingredient for any such improved model.

¹² In which spins are selected at random, and updated each time a halo doubles its mass, and which has been the standard option in GALACTICUS to date.

¹³ Note that, when computing the angular momentum of galactic discs (which is the primary determinant of their sizes), GALACTICUS currently ignores only utilizes information about the magnitude of the spin, ignoring the direction of the spin vector—i.e. it effectively assumes that the spin vector always points in the same direction when computing disc angular momentum. This is a simplification made by the model (since, until now, reliable spin vectors have not been available for the majority of halos), which we intend to improve upon as a result of the developments made in this present work. Correctly taking into account the vector nature of spin will likely also change the resulting distribution of disc sizes.

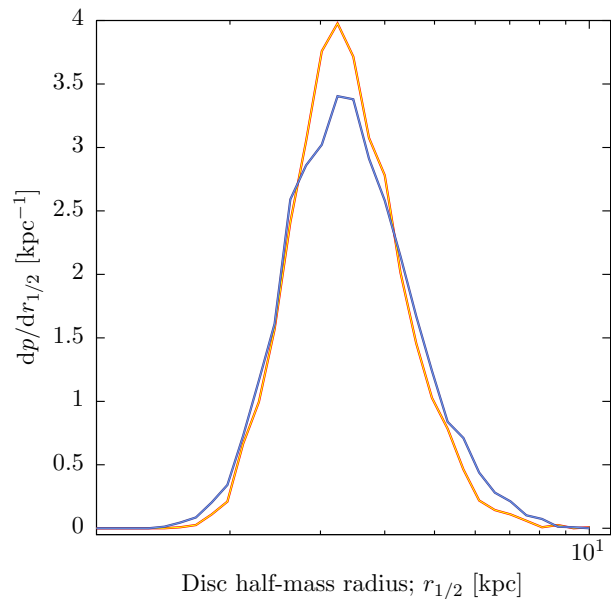


Figure 5. The distribution of half-mass radii of galactic discs in disc-dominated central galaxies occupying $2 \times 10^{12} M_{\odot}$ halos at $z = 0$ as computed using the GALACTICUS semi-analytic model. The yellow line shows results obtained using the Galform model for spins, in which spins are selected at random from a distribution, and updated each time a halo doubles its mass, while the blue line shows results when the model for spins developed in this work is used.

ACKNOWLEDGEMENTS

The Millennium Simulation databases used in this paper and the web application providing online access to them were constructed as part of the activities of the German Astrophysical Virtual Observatory (GAVO).

DATA AVAILABILITY

The data underlying this article are available in Zenodo, at <http://doi.org/10.5281/zenodo.3897353>. N-body simulation data from the Millennium Simulation is publicly available at <http://gavo.mpa-garching.mpg.de/MyMillennium/>.

REFERENCES

- An S.-H., Kim J., Moon J.-S., Yoon S.-J., 2020, arXiv e-prints, 2005, arXiv:2005.06479
 Bailin J., Steinmetz M., 2005, ApJ, 627, 647
 Barnes J., Efstathiou G., 1987, ApJ, 319, 575
 Benson A. J., 2012, NewA, 17, 175
 —, 2014, MNRAS, 444, 2599
 —, 2017a, MNRAS, 471, 2871
 —, 2017b, MNRAS, 467, 3454
 Benson A. J., Bower R., 2010, MNRAS, 405, 1573
 Benson A. J., Ludlow A., Cole S., 2019, MNRAS, 485, 5010
 Bett P., Eke V., Frenk C. S., Jenkins A., Helly J., Navarro J., 2007, MNRAS, 376, 215

Bett P., Eke V., Frenk C. S., Jenkins A., Okamoto T., 2010, MNRAS, 404, 1137

Bett P. E., Frenk C. S., 2012, MNRAS, 420, 3324

—, 2016, MNRAS, 461, 1338

Bryan S. E., Kay S. T., Duffy A. R., Schaye J., Dalla Vecchia C., Booth C. M., 2013, MNRAS, 429, 3316

Bullock J. S., Dekel A., Kolatt T. S., Kravtsov A. V., Klypin A. A., Porciani C., Primack J. R., 2001, ApJ, 555, 240

Chen D. N., Jing Y. P., Yoshikaw K., 2003, ApJ, 597, 35

Cole S., Lacey C., 1996, MNRAS, 281, 716

Cole S., Lacey C. G., Baugh C. M., Frenk C. S., 2000, MNRAS, 319, 168

Doroshkevich A. G., 1970, Astrophysics, 6, 320

Drakos N. E., Taylor J. E., Berrouet A., Robotham A. S. G., Power C., 2018, arXiv e-prints, arXiv:1811.12839

Fall S. M., Efstathiou G., 1980, MNRAS, 193, 189

Gelman A., Rubin D. B., 1992, Statistical Science, 7, 457

Gottlöber S., Yepes G., 2007, ApJ, 664, 117

Grubbs F., 1969, Technometrics, 11, 1

Hoyle F., 1949, in Problems in Cosmical Aerodynamics, Proceedings of the Symposium on the Motion of Gaseous Masses of Cosmical Dimensions, Central Air Documents Office Ohio

Jiang F., Dekel A., Kneller O., Lapiner S., Ceverino D., Primack J. R., Faber S. M., Macciò A. V., et al., 2018, arXiv e-prints, 1804, arXiv:1804.07306

—, 2019, MNRAS, 488, 4801

Jiang L., Cole S., Sawala T., Frenk C. S., 2015, MNRAS, 448, 1674

Johnson J. W., Maller A. H., Berlind A. A., Sinha M., Holley-Bockelmann J. K., 2019, MNRAS, 486, 1156

Lee C. T., Primack J. R., Behroozi P., Rodríguez-Puebla A., Hellinger D., Dekel A., 2016, MNRAS

—, 2018, MNRAS, 481, 4038

Lemson G., Virgo Consortium t., 2006, arXiv Astrophysics e-prints, arXiv:astro

Liao S., Gao L., Frenk C. S., Guo Q., Wang J., 2017, MNRAS, 470, 2262

Libeskind N. I., Hoffman Y., Knebe A., Steinmetz M., Gottlöber S., Metuki O., Yepes G., 2012, MNRAS, 421, L137

Lu Y., Mo H. J., Wechsler R. H., 2015, MNRAS, 446, 1907

Ludlow A. D., Bose S., Angulo R. E., Wang L., Hellwing W. A., Navarro J. F., Cole S., Frenk C. S., 2016, MNRAS, 460, 1214

Macciò A. V., Dutton A. A., van den Bosch F. C., Moore B., Potter D., Stadel J., 2007, MNRAS, 378, 55

Mo H. J., Mao S., White S. D. M., 1998, MNRAS, 295, 319

Morinaga Y., Ishiyama T., 2019, arXiv e-prints, 1912, arXiv:1912.11647

Navarro J. F., Frenk C. S., White S. D. M., 1997, ApJ, 490, 493

Parkinson H., Cole S., Helly J., 2008, MNRAS, 383, 557

Peebles P. J. E., 1969, ApJ, 155, 393

Porciani C., Dekel A., Hoffman Y., 2002, MNRAS, 332, 325

Rodríguez-Puebla A., Behroozi P., Primack J., Klypin A., Lee C., Hellinger D., 2016, MNRAS, 462, 893

Sharma S., Steinmetz M., Bland-Hawthorn J., 2012, ApJ, 750, 107

Sheth R. K., Mo H. J., Tormen G., 2001, MNRAS, 323, 1

Springel V., Wang J., Vogelsberger M., Ludlow A., Jenkins A., Helmi A., Navarro J. F., Frenk C. S., et al., 2008, MNRAS, 391, 1685

Springel V., White S. D. M., Jenkins A., Frenk C. S., Yoshida N., Gao L., Navarro J., Thacker R., et al., 2005, Nature, 435, 629

Stefansky W., 1972, Technometrics, 14, 469

Terr Braak C. J. F., 2006, Stat Comput, 16, 239

Trenti M., Smith B. D., Hallman E. J., Skillman S. W., Shull J. M., 2010, ApJ, 711, 1198

Vitvitska M., Klypin A. A., Kravtsov A. V., Wechsler R. H., Primack J. R., Bullock J. S., 2002, ApJ, 581, 799

White S. D. M., 1984, ApJ, 286, 38

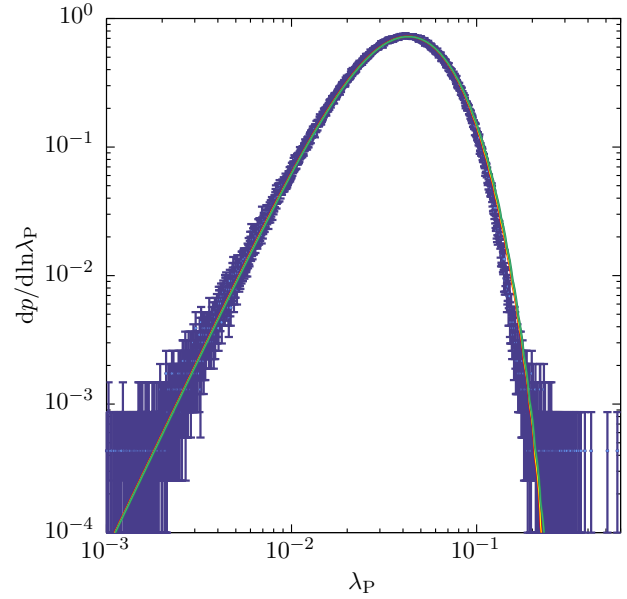


Figure A1. The distribution of spin parameters, λ_p , for relaxed halos at $z = 0$. The blue points with error bars show the results of Bett et al. (2007), while the lines show the results from our model for the maximum posterior probability model after convolution with the particle noise distribution predicted by the model of Benson (2017a) for merger tree resolutions of $M_{\text{res}} = 10^{-3} M_0$ (yellow line), and $M_{\text{res}} = 10^{-4} M_0$ (green line).

Zhang Y., Yang X., Faltenbacher A., Springel V., Lin W., Wang H., 2009, ApJ, 706, 747

Zjupa J., Springel V., 2017, MNRAS, 466, 1625

APPENDIX A: TREE RESOLUTION

Our merger trees are built with a mass resolution of $M_{\text{res}} = 10^{-3} M_0$. To test to what extent this finite resolution affects our results we run the maximum posterior probability model with $M_{\text{res}} = 10^{-4} M_0$. Figure A1 shows a comparison of this model with the standard resolution of $M_{\text{res}} = 10^{-3} M_0$ (yellow line), and with the higher resolution of $M_{\text{res}} = 10^{-4} M_0$ (green line). Using the higher resolution merger trees makes negligible difference to the resulting distribution. Specifically, we find that the distribution of spin parameters for λ_p shifts by less than 0.02 dex for $\lambda_p < 0.1$ relative to the $M_{\text{res}} = 10^{-3} M_0$ case, and shifts by less than 0.05 dex for $\lambda_p < 0.2$.

APPENDIX B: POSTERIOR DISTRIBUTION

Figure B1 shows the posterior distribution over the model parameters, with nuisance parameters not shown. Both parameters are well-constrained by the N-body data. It is also apparent that their values are strongly correlated in the posterior distribution.

The posterior distribution for α peaks at around $\alpha = 0.9$, with a tail extending to $\alpha \approx 3.0$. As the largest spins found for halos are $|\lambda| \approx 0.2$ this means that the largest value expected for $\alpha|\lambda_p| \approx 0.6 < 1$ such that the probability

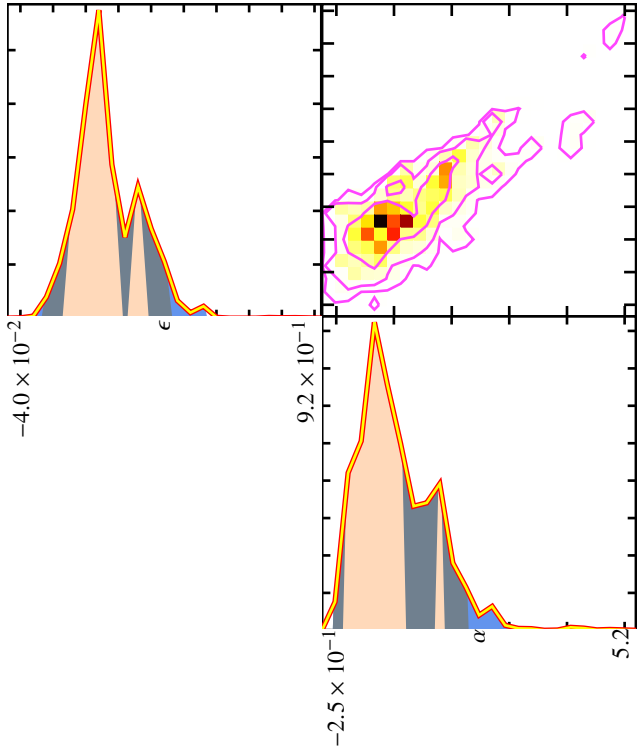


Figure B1. The posterior distribution over the model parameters ϵ and α . (Nuisance parameters are not shown.) The off-diagonal panel shows the posterior distribution over both model parameters, while on-diagonal panels show the posterior distribution over individual model parameters. In the off-diagonal panel, colours show the probability density running from white (low probability density) to dark red (high probability density). Contours are drawn to enclose 99.7%, 95.4%, and 68.3% of the posterior probability when ranked by probability density (i.e. the highest posterior density intervals). In on-diagonal panels the curve indicates the probability density. Shaded regions indicate the 68.3%, 95.4%, and 99.7% highest posterior density intervals.

distribution function described by equation (4) is always a valid distribution.

APPENDIX C: IMPLEMENTATION PSEUDOCODE

In this Appendix we provide an implementation of our algorithm for assigning spin parameters to halos in merger trees in pseudo-code, with citations to the relevant equations and source references. We do not describe the merger tree construction algorithm here, but focus solely on the algorithm for assigning spins. This spin algorithm is applicable to any well-formed merger tree. We use the following conventions:

tree: the merger tree being processed;
halo: the current halo being processed;
childHalo: a child (i.e. progenitor) halo of the current halo;
orbit: an object describing the orbit of a halo;
 $p_{\text{orbit}}()$: a distribution function for orbital parameters;
 $p_{\lambda}(\lambda)$: a distribution function for spin parameters;
 $p_{\Omega}()$: a distribution function for isotropically-distributed vectors;

$J_{\lambda}()$: the angular momentum as a function of spin parameter and halo properties;
 $J_{\text{subres}}()$: a function giving the angular momentum of sub-resolution halos;
 \leftarrow : implies assignment;
 \cdot *firstHalo*: an operator which returns the first halo for a depth-first walk of a merger tree;
 \cdot *firstChild*: an operator which returns the first child halo of a halo;
 \cdot *next*: an operator which returns the next halo in a depth-first walk of a merger tree, or *null* if no more halos remain;
 \cdot *sibling*: an operator which returns the next sibling of a halo (i.e. the next halo with the same parent as the operated on halo), or *null* if no next sibling exists;
 \cdot *sample*: an operator which samples from a distribution function.

Our implementation is as follows:

```

halo ← tree · firstHalo
while halo ≠ null do
  if halo · hasChildren then
    halo : J ← 0
    childHalo ← halo · firstChild
    while childHalo ≠ null do
      orbit ←  $p_{\text{orbit}}(\text{halo}, \text{childHalo}) \cdot \text{sample}$  (Jiang et al. 2015)
      halo : J ← halo : J + orbit · J + childHalo : J
      childHalo ← childHalo · sibling
    end while
    halo : J ← halo : J +  $J_{\text{subres}}(\text{halo})$  (eqn. 3)
  else
     $|\lambda| \leftarrow p_{\lambda}(\lambda) \cdot \text{sample}$  (Benson 2017a)
     $\hat{\lambda} \leftarrow p_{\Omega}() \cdot \text{sample}$ 
    halo : J ←  $J_{\lambda}(\lambda, \text{halo})$  (eqn. 1)
  end if
  halo ← halo · next
end while

```